Identification of Potent CD43+ Effector CD8+ T Cells Elicited After Transplantation

Gregory Cohen[1], Melissa Kallarakal[1], Francis Ibukun[1], Scott M. Krummey[1]*

[1]Department of Pathology, Johns Hopkins School of Medicine, Baltimore, MD

*Corresponding author, skrumme1@jhmi.edu

Keywords: MHC tetramer, $CD8^+$ T cell, costimulation blockade

ABSTRACT

$CD8^+$ T cells mediate acute rejection of allografts, which threatens the long-term survival of transplanted organs. After antigen encounter, $CD8^+$ T cells differentiate into effector populations that traffic to allografts and exert cytotoxic functions. The phenotype of effector $CD8^+$ T cells after transplantation is not well-understood. We characterized the use of an allogeneic MHC Class I tetramer comprised of the ubiquitous self-peptide QL9 presented by $H\text{-}2L^d$, to assess anti-donor H-2b $CD8^+$ T cells. T cells specific for this epitope were found at an elevated precursor frequency in naïve mice relative to nominal and viral antigens. After grafting of allogeneic $H\text{-}2^d$ skin, L^d $QL9^+$ T cells divided and differentiated into effector $CD8^+$ T cells, but only weakly increased in numbers. Antigen-specific effector $CD8^+$ T cells downregulated CD127, but a low frequency expressed the effector marker KLRG-1. Using high-parameter flow cytometry, we found that expression of the activated glycoform of sialophorin CD43 increased at acute timepoints. Relative to CD43- populations, effector $CD43^+$ $CD8^+$ T cells displayed potent effector phenotype and functionality, including GranzymeB production, cytokine production, and accelerated graft rejection. In the presence of costimulation blockade with CTLA-4 Ig, $CD43^+$ effector T cells maintained high expression of the costimulatory receptor ICOS. ICOS blockade in conjunction with CTLA-4 Ig prolonged graft survival. These data demonstrate that the graft-specific $CD8^+$ T cell response has a distinct response profile relative to anti-pathogen responses and that CD43 and ICOS are critical surface receptors that define potent effector $CD8^+$ T cell populations that form after grafting. These findings have implications for the selective targeting of $CD8^+$ T cells that mediate transplant rejection.

INTRODUCTION

The activation of $CD8^+$ T cells relies on the recognition of cognate antigen, costimulatory and coinhibitory receptor signaling, and the local profile of cytokines.[1–3] The balance of these factors shapes the magnitude and character of the $CD8^+$ T cell response. In transplantation, $CD8^+$ T cells can respond to allogeneic antigen presented on donor MHC Class I proteins and mediate tissue damage.[4,5] Recent clinical studies have highlighted that the occurrence of acute rejection has a cumulatively detrimental effect on the long-term survival of transplanted organs.[6–8]

Activated T cells undergo several well-established phenotypic changes that distinguish them from quiescent naïve $CD8^+$ T cells. The majority of the work underlying these paradigms has been performed in infection models, which present distinct profile of inflammation and antigen relative to transplanted organs.[9–11] The canonical phenotype of an effector $CD8^+$ T cell, $CD44^{hi}CD62L^{lo}$, does not specifically identify the responding allogeneic cells among the larger pool of previously activated $CD8^+$ T cells in an organism. Expression of the surface receptor KLRG-1 is also used to identify actively responding effector $CD8^+$ T cells relative to memory precursor cells.[12–14] However, KLRG-1 expression is both not functionally required for the effector function of $CD8^+$ T cells and not induced after all types of priming *in vivo*.[15] A recent report found very little KLRG-1 expression after grafting relative to a viral infection.[15] Thus, in order to more granularly understand anti-graft $CD8^+$ T cell responses and develop strategies to target the allogeneic response, deeper understanding of the differentiation program of post-graft $CD8^+$ T cells is needed.

CD43 is a transmembrane surface receptor on immune cells that has a wide range of immune cell types and has established intracellular signaling and cell adhesion functions. Expression of CD43 is uniformly high on T cells, but a larger activated glycoform, defined by the 1B11 epitope, is selectively expressed in certain contexts.[16] Multiple studies have shown that CD43 dampens T cell activation and is essential for optimal trafficking into inflamed tissues.[17–22]

CD43 expression on $CD8^+$ T cells is necessary for homeostatic contraction after viral infection and pathogenic autoimmune responses,[17,18] and CD43 (1B11) is expressed on a subset of memory $CD8^+$ T cells that have poor recall potential.[23] However, the impact of CD43 signaling and the role of activated CD43 (1B11) expression on $CD8^+$ T cell differentiation is not well-understood.

Due to the technical difficulties in identifying allogeneic epitopes, the $CD8^+$ T cell response is typically evaluated by using either TCR transgenic mice (e.g. OT-I/OVA) or evaluating bulk activated $CD8^+$ T cells. Both approaches sacrifice potential insights gained by assessing the acutely responding T cell clones in the context of physiologic antigen levels, precursor frequency, clonal competition, and inflammatory signals. MHC tetramers have provided a tremendous advance into the ability to identify and track antigen-specific $CD8^+$ T cell responses to pathogens and model antigens.[24–27] However, the use of MHC tetramers to study allogeneic T cells has been limited, due to the technical challenges of identifying appropriate epitopes from across the proteome.

In order to be able to study antigen-specific $CD8^+$ T cells in the context of fully-allogeneic transplant model, we sought to develop the use of allogeneic MHC Class I tetramers specific for an $H\text{-}2^d$ epitope that is recognized by $H\text{-}2^b$ C57Bl/6 $CD8^+$ T cells. Using elegant work performed in the characterization of the 2C TCR transgenic mouse model,[28–30] we were able to use MHC tetramer of an $H\text{-}2L^d$ restricted epitope for the epitope QL9 from a ubiquitously expressed metabolic enzyme. This approach allowed us to directly study the $CD8^+$ T cell response to fully allogeneic grafts and characterize the differentiation of effector populations in the context of physiologic antigen and inflammation. Here we report the characteristics of the $CD8^+$ T cell response to allogeneic antigen and the differentiation of a population of potent $CD43^+$ T_{EFF}.

METHODS

Mice. Male C57BL/6J and C57BL/6J Ly5.2-Cr (CD45.1) strains were obtained from The Jackson Laboratory (Bar Harbor, Maine) at 6-8 weeks of age. Balb/cJ and C57Bl/6-Tg(TcraTcrb)1100Mjb/J (OT-I) were obtained from The Jackson Laboratory and bred at Johns Hopkins. All transplant experiments were conducted in age-matched male hosts randomly assigned to experimental groups. This study was conducted in accordance with the recommendations in the Guide for the Care and Use of Laboratory Animals. The protocol was approved by the Animal Care and Use Committee at Emory University and Johns Hopkins University. Animals were housed in specific pathogen-free animal facilities at Emory University and Johns Hopkins University.

Skin Grafting. Full-thickness tail and ear skins were transplanted onto the dorsal thorax of recipient mice and secured with adhesive bandages as previously described.[31] In some experiments, mice were treated with 250 ug/dose of CTLA-4 Ig (BioXCell) and anti-ICOS (BioXCell) via i.p. injection on day 0, 2, 4, and 6.

MHC Tetramers and CD8$^+$ T cell Enrichment. MHC tetramers with human β2-microglobulin specific for QL9 (H-2L^d QLSPFPFDL) and OVA (H-2K^b SIINFEKL) were obtained from the NIH Tetramer Core facility. Tetramer enrichment was performed based on published protocols.[32] Briefly, single cell suspensions of splenocytes or lymphocytes were incubated with MHC tetramer (PE or APC), followed by incubation with anti-PE or anti-APC paramagnetic microbeads (Miltenyi), and enrichment over an LS column (Miltenyi). The column flow through was collected as the unbound fraction containing bulk CD8$^+$ T cells and the column bound fraction enriched for tetramer binding cells were stained for surface and intracellular antigens and analyzed by flow cytometry. Absolute cell counts were performed using CountBrite beads (BD Biosciences) or Cytek Aurora.

Antibodies and Flow Cytometry. Flow cytometry and magnetic enrichment were performed in 1X PBS (without Ca^{2+}/Mg^{2+}, pH 7.2), 0.25% BSA, 2 mM EDTA, and 0.09% azide. Sigle cell

suspensions were incubated in 96-well U-bottom plates with the following antibodies for 30-60 min at room temperature: CD4, CD8, CD11c, F4/80, CD19, CD27, CD28, CD127, KLRG-1, CD43, CXCR3, CD62L, ICOS, CD44, CD62L. Intracellular staining was performed using the Transcription Factor Staining Kit (eBiosciences) and the following antigens: Ki67, Nur77, GranzymeB, T-Bet, IFN-γ, TNF-α. Dead cells were excluded with Live/Dead Aqua (Invitrogen) or Live/Dead Near IR (Biolegend) according to manufacturer's instructions.

Ex vivo Allogeneic Stimulation for Cytokine Production. Splenocytes and draining lymph node cells from CD45.1+ mice grafted with Balb/c skin grafts 14 days prior were processed to single cell suspension and pooled. 1.5×10^6 CD45.1 cells were incubated with 2×10^6 Balb/c splenocytes in the presence of 1 mg/mL GolgiStop (Invitrogen) for 4-5 h. Cells were collected and gated on CD45.1$^+$ CD8$^+$ T cells for intracellular cytokine analysis.

FACS sorting and adoptive transfer. Splenocytes and draining lymph nodes cells from CD45.1$^+$ mice grafted with Balb/c skin grafts 10-14 days prior were stained to identify effector CD62L^{lo}CD43$^+$ and CD62L^{lo}CD43- CD8+ T cells. Cells were sorted on a MoFlo XDP. 9×10^5 purified cells were transferred via tail vein into C65Bl/6 mice. Mice were grafted the following day with Balb/c skin and monitored for graft survival.

***In vitro* OT-I Stimulation**. Naïve OT-I splenocytes were stained with CellTrace Violet (Invitrogen) according to the manufacturer's instructions and plated in 24 well tissue culture plates at 3×10^6/well in in the presence of OT-I peptide (GenScript) and the following cytokines: CpG (3.125 μg/mL, Invivogen), IFN-α (Biolegend, 1.1 μg/mL), IL-12 (Biolegend, 10 ng/mL), IL-15 (Biolegend, 10 ng/mL), IFN-γ (Biolegend, 100 ng/mL)

Cells were incubated in Complete R10 media comprised of RPMI 1640 with L-glutamine (Corning), 10% FBS, 100 mM HEPES, 500 uM β-mercaptoethanol, 100 U/mL penicillin/stremptomycin at 37 C (5% CO_2) for 72 h prior to analysis by flow cytometry.

Flow Cytometry Analysis. In all analysis, $CD8^+$ T cells were identified as singlet events, Live/Dead $stain^-$, dump $gate^-$ (CD11c, F4/80, NK1.1, CD19), $CD4^-$, $CD8^+$ events. Manual gating was performed in Flowjo 10. Tetramer and bulk $CD8^+$ T_{EFF} are defined as $CD44^{hi}CD8^+$ T cells. For dimensionality reduction analysis, manually gated unbound $CD8^+$ T cells and bound fraction L^d $QL9^+$ $CD8^+$ T cells events were imported into R (4.1.1) through CytoML (2.40), flowWorkspace (4.4.0), and flowCore (2.4.0). Markers were transformed by hyperbolic arcsine with a cofactor of either 1000 or 6000 depending on the marker. The data were further analyzed using CATALYST (1.16.2) with FlowSOM (2.0.0) clustering and ConsensusClusterPlus (1.56.0) meta clustering. UMAP dimensionality reductions were generated with scatter (1.20.1). Visualizations were generated in ggplot2 (3.3.5) and ComplexHeatmap (2.8.0).

Statistical Analysis. All data points represent individual donors, and where individual data points are not depicted the value of n is provided in the corresponding figure legend. For analysis of absolute numbers and expression levels, paired or unpaired Student's t-tests (two-tailed) were performed where appropriate. In vitro CD43 and Nur77 expression data was normalized to the maximum MFI obtained for each marker in a given experiment. Error bars represent standard error measurements (SEM). Statistics were performed using GraphPad Prism 9. Significance was determined as *$p<0.05$, **$p<0.01$, ***$p<0.001$, ****$p<0.0001$.

RESULTS

MHC Class I tetramer can be used to identify L^d $QL9^+$ $CD8^+$ T cells in naïve C57Bl/6 mice

The 2C TCR has been characterized to identify an H-$2L^d$ restricted peptides for α-ketoglutarate dehydrogenase[28–30]. We hypothesized that MHC tetramers of this epitope could be used to identify endogenous alloreactive $CD8^+$ T cells. In order to reliably detect rare $CD8^+$ T cells, we incubated single cell suspensions with L^d QL9 tetramers and enriched with magnetic beads specific for the fluorophore of the tetramer **(Figure 1A)**[33]. This creates a tetramer enriched (column "bound") and bulk $CD8^+$ (column "unbound") fractions of cells for analysis.

In naïve C57Bl/6 mice, we detected a population of L^d QL9 tetramer binding cells using PE and APC tetramers **(Figure 1B)**. Using this approach, we identified L^d QL9 and K^b OVA-specific $CD8^+$ T cells in the spleen and draining lymph nodes **(Figure 1C)**. Tetramer binding was specific as no L^d QL9 binding cells were found in OT-I RAG1 KO mice (Figure 1C). The precursor frequency of K^b OVA $CD8^+$ T cells was significantly lower than that of L^d QL9 $CD8^+$ T cells **(Figure 1D and 1E)**. The phenotype of L^d QL9 binding $CD8^+$ T cells was largely $CD44^{lo}CD62L^{hi}$, similar to the bulk $CD8^+$ T cell population in the mice **(Figure 1F-G)**. Thus, the L^d QL9 tetramer specifically binds to a population of naïve $CD8^+$ T cells that appear to be at a relatively elevated precursor frequency versus the nominal antigen K^b OVA.

L^d $QL9^+$ $CD8^+$ T cells become activated and proliferate after H-2^d Balb/c skin grafts

In order to evaluate whether naïve L^d $QL9^+$ $CD8^+$ T cells responded when presented with allogeneic H-$2L^d$ antigen, we performed skin grafts of H-2^d Balb/c mice onto C57Bl/6 mice and assessed tetramer binding $CD8^+$ T cells **(Figure 2A)**. We found that a significant portion of L^d $QL9^+$ $CD8^+$ T cells became $CD44^{hi}$ on day 10 after skin grafting in the draining lymph nodes and spleen (Figure 2B), indicating activation after exposure to antigen. The absolute number of $CD44^{hi}$ L^d QL9 tetramer binding cells increased on day 10 in both the draining lymph nodes and spleen

(Figure 2C), representing an average change of 10-fold in the draining lymph node and 6.1-fold in the spleen **(Figure 2D)**.

In order to assess whether the phenotypic and cell number changes represented a proliferative response in L^d QL9-specific $CD8^+$ T cells, we stained cells for Ki67 in order to assess proliferation and evaluated $CD8^+$ T cells over time after Balb/c skin grafting. We found that in both the draining lymph node and spleen, the frequency of $Ki67^+$ cells increased at day 4 and 7, and on day 10 nearly all of the L^d $QL9^+$ $CD44^{hi}$ $CD8^+$ T cells were $Ki67^+$ in both the draining lymph nodes and spleen **(Figure 2E and 2F)**. Thus, the L^d QL9 tetramer identifies a population of $CD8^+$ T cells that increase in absolute numbers, become activated and proliferative after Balb/c skin grafting.

A low frequency of $CD8^+$ T_{EFF} express KLRG-1^+ after grafting

We next wanted to determine the phenotypic profile of the L^d $QL9^+$ effector CD8+ T cells (T_{EFF}, as defined by $CD44^{hi}$ status) after grafting. The early $CD8^+$ T cell response is most often defined by the reciprocal expression of the CD127 (IL-7Rα) and KLRG-1 receptors. In the first 1-2 weeks after infection, a significant portion (50-70%) of T_{EFF} upregulate KLRG-1^+,[14,34,35] and these cells are short-lived and display potent effector functions. We assessed the expression of CD127 and KRLG-1 using L^d QL9 tetramers after grafting in both the spleen and draining lymph nodes **(Figure 3)**. In response to a Balb/c skin graft, some $CD127^{lo}$ and $KLRG1^+$ T_{EFF} cells were induced, with a peak frequency at day 10 that declined at day 21 and 43. However, even among L^d $QL9^+$ cells, KLRG-1^+ T_{EFF} represented 5-10% of the T_{EFF} in the draining lymph nodes and spleen. Thus, even among L^d $QL9^+$ cells that are specific for graft antigen, and represent a highly proliferative population, KLRG-1 expression is not a dominant phenotype after grafting.

Activated CD43 glycoform expression is induced on a population of $CD8^+$ T_{EFF} after grafting

To better characterize the phenotypes of the $CD8^+$ T_{EFF} cells after grafting, we devised a high-parameter flow cytometry panel with canonical costimulatory receptors as well as activation and proliferation markers. We evaluated L^d $QL9^+$ and bulk $CD8^+$ T cells on day 0, 10, 21, and 42 after Balb/c skin grafting. We clustered these populations with FlowSOM and ConsensusClusterPlus and visualized with UMAP dimensionality reduction **(Figure 4A)**. We evaluated the frequency of clusters and found four clusters with enriched frequencies on day 10, and three that were enriched on day 21-42 **(Figure 4B-C)**. We evaluated Day 10 enriched clusters, as these fit the kinetic profile of a short-lived effector population. All four Day 10 Clusters were $CD44^{hi}$, $Ki67^+$, $CXCR3^{hi}$ and $KLRG\text{-}1^-$ **(Figure 4D)**. Interestingly, these clusters varied most in expression of CD62L and the activated glycoform of CD43 (identified by the antibody clone 1B11). While Day 10 Clusters 1 and 2 were $CD62L^{hi}CD43^-$, Cluster 3 was $CD62L^{lo}CD43^-$, and Cluster 4 was $CD62L^{lo}CD43^+$ (**Figure 4D).** Thus, these two surface receptors appear to represent dynamically changing populations within the anti-graft T_{EFF} pool. In order to evaluate the expression of CD62L and CD43 after grafting, we performed manual gating on L^d $QL9^+$ and bulk $CD8^+$ T_{EFF}. We found that the frequency of $CD62L^{lo}CD43^+$ T_{EFF} increased at day 10 and 21 and declined to a memory timepoint **(Figure 4E)**. Thus, anti-graft $CD43^+$ T_{EFF} represents a short-lived phenotype that after grafting.

$CD43^+$ $CD8^+$ T_{EFF} display potent effector functions relative to $CD43^-$ T_{EFF} populations. We next wanted to assess whether $CD43^+$ T_{EFF} displayed competent effector functions relative to $CD43^-$ T_{EFF} populations. We grafted C57Bl/6 mice with Balb/c skin and assessed $CD8^+$ T cells during the peak effector response (day 10-14; **Figure 5A**). We found that among the L^d $QL9^+$ cells, $CD43^+$ T_{EFF} expressed significantly higher levels of both GranzymeB and T-BET as compared with $CD62L^{hi}$ or $CD62L^{lo}$ $CD43^-$ T_{EFF} populations **(Figure 5B-C)**. We assessed the capacity of these populations for cytokine production by stimulating $CD45.1^+$ T_{EFF} *ex vivo* with

Balb/c splenocytes, and found that $CD43^+$ T_{EFF} produced nearly all of the IFN-γ and TNF-α, and that the majority of these cells were double producers **(Figure 5D)**.

We wanted to assess whether the effector phenotype corresponded with an enhanced potency to mediate graft rejection *in vivo*. To isolate the impact of CD43 on T_{EFF}, we FACS-sorted $CD44^{hi}$ $CD8^+$ T cells into $CD43^+$ and $CD43^-$ T_{EFF} ($CD62L^{lo}$) on day 10-14 and adoptively transferred $9x10^5$ cells into C57Bl/6 mice who were subsequently grafted with Balb/c skin. We found that the $CD43^+$ T_{EFF} group rejected skin grafts with significantly faster kinetics than $CD43^-$ T_{EFF} group **(Figure 5F)**, demonstrating the impact of $CD43^+$ T_{EFF} to mediate potent graft rejection. Overall, these data demonstrate that $CD43^+$ T_{EFF} are potent population of effector $CD8^+$ T cells *in vivo*.

CD43 expression is selectively induced by Type I interferon. Multiple studies have evaluated the impact of inflammation on the development and function of $CD8^+$ T cell populations[14,36]. However, the role of individual cytokines has not been well-established. We questioned whether the induction of CD43 expression was due to specific cytokine signaling or a pleiotropic effect of inflammation. We activated OT-I T cells *in vitro* in the presence of individual inflammatory cytokines **(Figure 5G)**. We used CellTrace Violet to assess the proliferation status of cells in culture. We included expression of Nur77, an orphan nuclear receptor whose expression level reflects the cumulative strength of antigen stimulation[37,38], as a control for the overall level of activation of the cells in the presence of cytokines. We found that antigen stimulation induced CD43 and Nur77 expression **(Figure 5H)**. The TLR9 agonist CpG, which has been shown to induced CD43 (1B11) expression[39], increased CD43 expression further than antigen stimulation alone. Among inflammatory cytokines, we found that only IFN-α induced CD43 expression, while IFN-γ, IL-15, and IL-12 did not have an effect versus antigen stimulation alone **(Figure 5H)**. The expression of Nur77 was not significantly impacted by the provision of any inflammatory cytokine.

These results demonstrate that CD43 (1B11) expression is induced by Type I IFN mediated signaling.

Costimulation blockade with CTLA-4 Ig does not inhibit CD8$^+$ T cells. We next evaluated the impact of CD28 costimulation blockade with CTLA-4 Ig. We treated mice with CTLA-4 Ig in compared to a control untreated group and analyzed CD8$^+$ T cells on day 10 after grafting with Balb/c skin grafts **(Figure 6A)**. In order to evaluate the phenotype of CD8$^+$ T cells in the presence of CTLA-4 Ig, we performed UMAP analysis of L^d QL9$^+$ and bulk CD8$^+$ T cells in treated and control mice **(Figure 6B)**. We found four clusters that were CD44^{hi} T_{EFF} and evaluated the expression of costimulation receptors, activation markers, and functional markers **(Figure 6B-D)**. CD44^{hi} Clusters 2 and 3 had high CD43 (1B11) expression, and were also CD62L^{lo}, CXCR3^{hi}, and Ki67$^+$. Interestingly, both had high expression of the costimulation receptor ICOS (Figure 6D). Using manual gating, we evaluated whether the frequency of CD62L and CD43 T_{EFF} was impacted by CTLA-4 Ig treatment, and found that all three populations were similar between groups **(Figure 6E)**. We next evaluated ICOS expression on CD43 vs CD62L T_{EFF}, and found that ICOS expression was almost exclusively found on CD62L^{lo}CD43$^+$ T_{EFF} **(Figure 6F)**. In order to assess whether ICOS costimulation provisioned functional signals in the context of graft rejection, we assessed the impact of ICOS blockade in combination with CTLA-4 Ig treatment. We found that anti-ICOS prolonged graft survival versus CTLA-4 Ig alone **(Figure 6G)**. Thus, ICOS represents a functional costimulation target that can be used to inhibit CTLA-4 Ig resistant CD8$^+$ T cells.

DISCUSSION

In this study, we characterized the alloimmune effector CD8+ T cell response against the H-2L^d-restricted epitope QL9. We found that the precursor frequency for L^d QL9$^+$ T cells is elevated compared with K^b OVA and the published frequencies of pathogen-specific antigens.[24–27] Based on multiple studies using primarily proliferation assays, the precursor frequency for alloimmune responses has been described as elevated relative to protective immune responses.[5,40] However, to our knowledge this is the first demonstration of this finding using MHC tetramers to directly visualize allogenic epitope-specific CD8$^+$ T cells.

We found that at the peak of the immune response, the majority of L^d QL9$^+$ T cells become CD44^{hi}, nearly all CD44^{hi} L^d QL9$^+$ T cells are Ki67$^+$, providing strong evidence that the tetramer binding T cells are recognizing endogenously presented L^d QL9 on grafts. While the QL9 peptide is a single amino acid extension of the parent 2C peptide, prior studies investigating the peptides recognized by the 2C TCR speculated that the QL9 was not detected due to technical limitations of peptide sequencing in acidic conditions.[28,29] This work provides evidence that QL9 is an endogenously presented peptide in the context of H-2L^d.

Effector CD8$^+$ T cells differentiate into distinct subsets based on the combination of antigen, costimulation, and inflammatory signals that are present. In contrast to pathogen-specific CD8$^+$ T cell responses at acute timepoints, we found that very few effector CD8$^+$ T cells expressed KLRG-1 after grafting. This highlights that the allogeneic priming environment has phenotypic consequences in shaping CD8$^+$ T cell responses, and led us to carefully evaluate the post-graft CD8$^+$ T cell programming. Using a high-parameter flow cytometry panel to evaluate activation, costimulation, and proliferation markers, we found that a subset of L^d QL9$^+$ T_{EFF} express the activated glycoform of CD43 (1B11 clone). The frequency CD43$^+$ T_{EFF} increased acutely after transplant and these cells were potently cytotoxic relative to CD43$^-$ T_{EFF} populations.

CD43 is a transmembrane receptor with recognized intracellular signaling and adhesion functions.[17,19,21] Studies evaluating the role of CD43 in disease models have found varying and sometimes conflicting consequences. CD43 deficient $CD8^+$ T cells have been found to undergo a decreased rate of apoptosis during the contraction phase of the response to a virus,[17] but including increased levels of apoptosis in a model of sepsis.[41] Multiple studies have shown that CD43 is critical for trafficking into peripheral tissues.[17,19,22,42] Of note, the majority of studies have evaluated the function of the receptor versus knockout, less is known about the functional impact of CD43 1B11 expression on T cells. Future studies will have to evaluate the importance of CD43 1B11 expression on the function of T_{EFF} in the context of transplant, including the ability to traffic within secondary lymphoid tissue and into allografts.

We evaluated antigen-specific T_{EFF} in the presence of costimulation blockade with CTLA-4 Ig, and found that the costimulatory receptor ICOS is selectively expressed on $CD43^+$ T_{EFF}. Blockade of ICOS prolonged graft survival, indicating that ICOS plays a functional role in the presence of CTLA-4 Ig treatment. ICOS has been implicated as an important costimulatory receptor in multiple T cell subsets, and was recently shown to be important for the formation of resident memory $CD8^+$ T cells. ICOS is attractive as a therapeutic target because it is selectively upregulated on $CD43^+$ T_{EFF}, and thus represents a potentially selective way to inhibit allogeneic $CD8^+$ T cells during rejection. Currently, ICOS blocking agents are in pre-clinical development for multiple diseases.[43,44]

Overall, by using a novel MHC tetramer-based approach, this study provides new insight into the characteristics of the alloimmune $CD8^+$ T cell response, including the identification of a potent T_{EFF} phenotype. Future studies are needed to investigate the translational potential of these findings to inhibit graft-specific $CD8^+$ T cells in transplant patients.

ACKNOWLEDGEMENTS

We thank members of the Ford Lab and the Immunology Division of the Department of Pathology for helpful discussions. We appreciate Hao Zhang and the Bloomberg School of Public Health Flow Cytometry and Cell Sorting Core for excellent cell sorting, and the NIH Tetramer Core Facility for tetramer reagents and technical advice. This work was supported by K99/R00 NIAID AI46271 (S.M.K) and the Transplant Immunology Research Network Fellowship Grant (S.M.K.).

REFERENCES

1. Jameson, S. C. & Masopust, D. Understanding Subset Diversity in T Cell Memory. *Immunity* **48**, 214–226 (2018).
2. Chung, H. K., McDonald, B. & Kaech, S. M. The architectural design of CD8+ T cell responses in acute and chronic infection: Parallel structures with divergent fates. *Journal of Experimental Medicine* **218**, (2021).
3. Ford, M. L. T Cell Cosignaling Molecules in Transplantation. *Immunity* **44**, (2016).
4. Callemeyn, J. *et al.* Allorecognition and the spectrum of kidney transplant rejection. *Kidney International* (2021) doi:10.1016/j.kint.2021.11.029.
5. Felix, N. J. *et al.* Alloreactive T cells respond specifically to multiple distinct peptide-MHC complexes. *Nature Immunology* **8**, 388–397 (2007).
6. Cherukuri, A. *et al.* Transitional B cell cytokines predict renal allograft outcomes. *Science Translational Medicine* **13**, (2021).
7. Meier-Kriesche, H.-U. *et al.* Increased Impact of Acute Rejection on Chronic Allograft Failure in Recent Era. *Transplantation* **70**, (2000).
8. Cole, E. H., Johnston, O., Rose, C. L. & Gill, J. S. Impact of Acute Rejection and New-Onset Diabetes on Long-Term Transplant Graft and Patient Survival. *Clinical Journal of the American Society of Nephrology* **3**, (2008).
9. Dwyer, G. K. & Turnquist, H. R. Untangling Local Pro-Inflammatory, Reparative, and Regulatory Damage-Associated Molecular-Patterns (DAMPs) Pathways to Improve Transplant Outcomes. *Frontiers in Immunology* **12**, (2021).
10. Colvin, M. M., Smith, C. A., Tullius, S. G. & Goldstein, D. R. Aging and the immune response to organ transplantation. *Journal of Clinical Investigation* **127**, 2523–2529 (2017).

11. Braza, F., Brouard, S., Chadban, S. & Goldstein, D. R. Role of TLRs and DAMPs in allograft inflammation and transplant outcomes. *Nature Reviews Nephrology* **12**, 281–290 (2016).

12. Sarkar, S. *et al.* Functional and genomic profiling of effector CD8 T cell subsets with distinct memory fates. *Journal of Experimental Medicine* **205**, 625–640 (2008).

13. Herndler-Brandstetter, D. *et al.* KLRG1+ Effector CD8+ T Cells Lose KLRG1, Differentiate into All Memory T Cell Lineages, and Convey Enhanced Protective Immunity. *Immunity* **48**, 716-729.e8 (2018).

14. Joshi, N. S. *et al.* Inflammation Directs Memory Precursor and Short-Lived Effector CD8+ T Cell Fates via the Graded Expression of T-bet Transcription Factor. *Immunity* **27**, (2007).

15. Bozeman, A. M., Laurie, S. J., Haridas, D., Wagener, M. E. & Ford, M. L. Transplantation preferentially induces a KLRG-1lo CD127hi differentiation program in antigen-specific CD8+ T cells. *Transplant Immunology* **50**, (2018).

16. Clark, M. C. & Baum, L. G. T cells modulate glycans on CD43 and CD45 during development and activation, signal regulation, and survival. *Ann N Y Acad Sci* **1253**, 58–67 (2012).

17. Onami, T. M. *et al.* Dynamic Regulation of T Cell Immunity by CD43. *The Journal of Immunology* **168**, 6022–6031 (2002).

18. Ford, M. L. & Evavold, B. D. Modulation of MOG 37–50-specific CD8+ T cell activation and expansion by CD43. *Cellular Immunology* **240**, 53–61 (2006).

19. Mody, P. D. *et al.* Signaling through CD43 regulates CD4 T-cell trafficking. *Blood* **110**, 2974–2982 (2007).

20. Cannon, J. L. *et al.* CD43 Regulates Th2 Differentiation and Inflammation. *The Journal of Immunology* **180**, 7385–7393 (2008).

21. Sperling, A. I. *et al.* CD43 is a murine T cell costimulatory receptor that functions independently of CD28. *Journal of Experimental Medicine* **182**, 139–146 (1995).

22. Cannon, J. L. *et al.* CD43 interaction with ezrin-radixin-moesin (ERM) proteins regulates T-cell trafficking and CD43 phosphorylation. *Molecular Biology of the Cell* **22**, 954–963 (2011).

23. Hikono, H. *et al.* Activation phenotype, rather than central– or effector–memory phenotype, predicts the recall efficacy of memory CD8+ T cells. *Journal of Experimental Medicine* **204**, 1625–1636 (2007).

24. Obar, J. J., Khanna, K. M. & Lefrançois, L. Endogenous Naive CD8+ T Cell Precursor Frequency Regulates Primary and Memory Responses to Infection. *Immunity* **28**, 859–869 (2008).

25. Kotturi, M. F. *et al.* Naive Precursor Frequencies and MHC Binding Rather Than the Degree of Epitope Diversity Shape CD8 $^{+}$ T Cell Immunodominance. *The Journal of Immunology* **181**, 2124–2133 (2008).

26. Haluszczak, C. *et al.* The antigen-specific CD8+ T cell repertoire in unimmunized mice includes memory phenotype cells bearing markers of homeostatic expansion. *Journal of Experimental Medicine* **206**, 435–448 (2009).

27. Jenkins, M. K. & Moon, J. J. The Role of Naive T Cell Precursor Frequency and Recruitment in Dictating Immune Response Magnitude. *The Journal of Immunology* **188**, 4135–4140 (2012).

28. Sykulev, Y. *et al.* High-affinity reactions between antigen-specific T-cell receptors and peptides associated with allogeneic and syngeneic major histocompatibility complex class I proteins. *Proceedings of the National Academy of Sciences* **91**, 11487–11491 (1994).

29. Chen, J., Eisen, H. N. & Kranz, D. M. A model T-cell receptor system for studying memory T-cell development. *Microbes and Infection* **5**, 233–240 (2003).

30. Udaka, K., Tsomides, T. J. & Eisen, H. N. A naturally occurring peptide recognized by alloreactive CD8+ cytotoxic T lymphocytes in association with a class I MHC protein. *Cell* **69**, 989–998 (1992).

31. Trambley, J. *et al.* Asialo GM1+ CD8+ T cells play a critical role in costimulation blockade–resistant allograft rejection. *Journal of Clinical Investigation* **104**, 1715–1722 (1999).

32. Moon, J. J. *et al.* Tracking epitope-specific T cells. *Nature Protocols* **4**, 565–581 (2009).

33. Moon, J. J. *et al.* Naive CD4+ T Cell Frequency Varies for Different Epitopes and Predicts Repertoire Diversity and Response Magnitude. *Immunity* **27**, 203–213 (2007).

34. Milner, J. J. *et al.* Delineation of a molecularly distinct terminally differentiated memory CD8 T cell population. *Proceedings of the National Academy of Sciences* **117**, 25667–25678 (2020).

35. Herndler-Brandstetter, D. *et al.* KLRG1+ Effector CD8+ T Cells Lose KLRG1, Differentiate into All Memory T Cell Lineages, and Convey Enhanced Protective Immunity. *Immunity* **48**, 716-729.e8 (2018).

36. Richer, M. J. *et al.* Inflammatory IL-15 is required for optimal memory T cell responses. *Journal of Clinical Investigation* **125**, 3477–3490 (2015).

37. Krummey, S. M. *et al.* Low-Affinity Memory CD8 $^{+}$ T Cells Mediate Robust Heterologous Immunity. *The Journal of Immunology* **196**, 2838–2846 (2016).

38. Moran, A. E. *et al.* T cell receptor signal strength in Treg and iNKT cell development demonstrated by a novel fluorescent reporter mouse. *Journal of Experimental Medicine* **208**, 1279–1289 (2011).

39. Nolz, J. C. & Harty, J. T. IL-15 regulates memory CD8+ T cell O-glycan synthesis and affects trafficking. *Journal of Clinical Investigation* **124**, 1013–1026 (2014).

40. Amir, A. L. *et al.* Allo-HLA reactivity of virus-specific memory T cells is common. *Blood* **115**, 3146–3157 (2010).

41. Fay, K. T. *et al.* Increased mortality in CD43-deficient mice during sepsis. *PLOS ONE* **13**, e0202656 (2018).

42. Ford, M. L., Onami, T. M., Sperling, A. I., Ahmed, R. & Evavold, B. D. CD43 Modulates Severity and Onset of Experimental Autoimmune Encephalomyelitis. *The Journal of Immunology* **171**, 6527–6533 (2003).

43. Solinas, C., Gu-Trantien, C. & Willard-Gallo, K. The rationale behind targeting the ICOS-ICOS ligand costimulatory pathway in cancer immunotherapy. *ESMO Open* vol. 5 (2020).

44. Adom, D. *et al.* ICOSL $^{+}$ plasmacytoid dendritic cells as inducer of graft-versus-host disease, responsive to a dual ICOS/CD28 antagonist. *Science Translational Medicine* **12**, (2020).

FIGURE LEGENDS

Figure 1. H-2L^d QL9 tetramers identify a population of naive CD8$^+$ T cells. (A) Single cell suspensions of lymph node or spleen tissue were incubated with MHC Class I tetramers, and enriched using magnetic beads specific for the tetramer fluorphores, creating a column bound tetramer enriched and unbound bulk CD8+ T cell fractions for analysis. (B) Representative flow cytometry plots and summary data depicting the frequency of CD8$^+$ T cells binding to one or both of the Ld QL9 PE or L^d QL9 APC tetramers in the bound or unbound fractions. (C) Representative flow cytometry plots of L^d QL9 and K^b OVA tetramer staining in naive C57Bl6 spleen and lymph nodes, or OT-I RAG1$^{-/-}$ spleen. (D) Absolute numbers of K^b OVA and L^d QL9 tetramer bindings CD8$^+$ T cells in the lymph nodes and spleen of naive C57Bl/6 mice. (E) Number of tetramer binding cells in the combined spleen and lymph nodes per million CD8+ T cells. (F) Representative flow cytometry plots depicting the phenotype of L^d QL9 tetramer binding CD8$^+$ T cells in the lymph nodes and spleen. (G) Summary data of the quadrant gating depicted in (F). Each point depicts an individual mouse. Summary data depicts pooled data from (B) 3 independent experiments (n=6/group), (D-E) 2 independent experiments (n=12/group), (F) 2 independent experiments (n=9/group). Statistical analysis performed by (D) 2-way ANOVA with Sidak's multiple comparisons test, (E) Student's unpaired t-test (2-tailed). Error bars depict SEM. *$p<0.05$, ***$p<0.001$, ****$p<0.0001$.

Figure 2. H-L^d QL9$^+$ CD8$^+$ T cells proliferate after grafting. (A) C57Bl/6 mice were grafted with H-2^d Balb/c skin. (B) Representative flow cytometry plots and (C) absolute numbers of CD8$^+$ T cells on day 0 or day 10 after grafting in the draining lymph nodes and spleen. (D) Fold change of the number of L^d QL9$^+$ CD8$^+$ T cells on day 10 post-graft relative to day 0 in the draining lymph nodes or spleen. (E-F) Representative flow cytometry plots and summary data of Ki67 staining among CD44hi CD8+ T cell populations in the (E) draining lymph nodes and (F) spleen. Each

data point depicts an individual mouse. Summary data depicts pooled data from (C-D) 4 independent experiments (n=12-17/group), (E-F) 2-3 independent experiments (6-9/group). Statistical analysis performed using (C) unpaired Student's t-test (2-tailed). Error bars depict SEM. *p<0.05, **p<0.01.

Figure 3. A low frequency of post-graft CD8$^+$ T cells express KLRG-1. C57Bl/6 mice were grafted with H-2d Balb/c skin and the frequency of L^d QL9$^+$ and bulk CD8$^+$CD44^{hi} CD127^{lo}KLRG-1$^+$ cells were quantified in the (A) draining lymph nodes and (B) spleen. Each data point depicts an individual mouse. Summary data depicts pooled results from from 2-3 independent experiments (n=6-12 mice/group). Error bars depict SEM.

Figure 4. CD8$^+$ T cells differentiate into CD43+ T effector populations that peak early after grafting. C57Bl/6 mice were grafted with H-2^d Balb/c skin and the frequency of L^d QL9$^+$ and bulk CD8$^+$ T cells were assessed in the spleen at the indicated timepoints. (A) UMAP of costimulation and activation markers from day 0, 10, 21, and 42 post-graft CD8$^+$ T cell populations. (B) Box plots of the frequency of clusters elevated at day 10 or day 21/42. (C) UMAP depicting day 10 and day 21/42 enriched clusters. (D) Histograms depicting expression of individual markers in day 10 and day 21/42 enriched clusters. (E) Expression of CD43 and CD62L on CD8$^+$ T cell populations at day 0, 10, 21, and 42 post-graft. Each data point depicts an individual mouse. Summary data depicts pooled data from (A-D) one (n=4 mice/group), (E) 2-3 independent experiments (n=5-10 mice/group). Statistics performed by (E) 1-way ANOVA. Error bars depict SEM *p<0.05, **p<0.01.

Figure 5. CD43$^+$ T$_{EFF}$ display potent effector function and mediate graft rejection. (A) C57Bl/6 mice were grafted with H-2^d Balb/c skin and L^d QL9$^+$ and bulk CD8$^+$ T cells were assessed

in the spleen at day 10-14 post-graft. The frequency of (B) Granzyme B+ cells and (C) T-BET+ cells in the indicated populations was assessed. (D) Post-graft effectors were stimulated in vitro for 5 hours with Balb/c splenocytes and the frequency of IFN-g and TNF-a producing cells was assessed. (E) Day 10-14 CD45.1+ CD8+ T cells were FACS sorted into CD62Llo CD43+ and CD43- populations and 9x105 cells/mouse were transferred into congenic hosts that were grafted with Balb/c skin grafts and assessed for survival. (F) Graft survival analysis of C57Bl/6 hosts transferred with CD45.1+ CD8+ T cell populations described in (E). (G) OT-I CD8+ T cells were labeled with CellTrace Violet and stimulated in vitro for 3 days in the presence of 0 uM (unstimulated) or 1 uM OVA peptide or the indicated cytokine. (H) Histograms depicting the expression of CD43 and Nur77 on undivided unstimulated or 1 uM peptide divided populations. For each individual experiment, the MFI was normalized to the maximum value of CD43 or Nur77. Each data point depicts an individual mouse. Summary data depicts pooled results from (B-D) 2 independent experiments (n=5-8 mice/group), (F) 2 independent experiments (n=7-15/group), (H) 3 independent experiments with an individual mouse. Statistical analysis performed by (B-D) 1-way ANOVA with Tukey's multiple comparisons test, (F) Log-rank (Mantel-Cox) test, (H) 2-way ANOVA with Dunnett's multiple comparisons test. Error bars depict SEM. *$p<0.05$, **$p<0.01$, ****$p<0.0001$.

Figure 6. ICOS expression is induced on CD43+ T_{EFF} and ICOS blockade prolongs graft survival. (A) Experimental schematic depicting the treatment of C57Bl/6 mice grafted with H-2^d Balb/c skin and treated with CTLA-4 Ig. (B) UMAP expression analysis of day 10 post-graft L^d/QL9-specific and bulk CD8+ T cells in the spleen in mice untreated or treated with CTLA-4 Ig. (C) UMAP depicting four $CD44^{hi}$ clusters. (D) Histograms of proteins used in UMAP analysis for four $CD44^{hi}$ clusters and the average of all samples. (E) Expression of CD62L and CD43 in the spleen on day 10 post-graft in mice as in (A). (F) Expression of ICOS on $CD8^+$ T_{EFF} populations in CTLA-4 Ig and control mice. (G) Graft survival of C57Bl/6 mice treated with CTLA-4 Ig or CTLA-

4 Ig with anti-ICOS and grafted with a Balb/c skin graft. Each data point depicts an individual mouse. Summary data depicts pooled results from (E-F) 2 independent experiments (n=6-7 mice/group), (G) 3 independent experiments (n=12-16/group). Statistical analysis performed by (E-F) 2-way ANOVA with Tukey's multiple comparisons test, (G) Log-rank (Mantel-Cox) test. Error bars depict SEM. **$p<0.01$

Figure 1

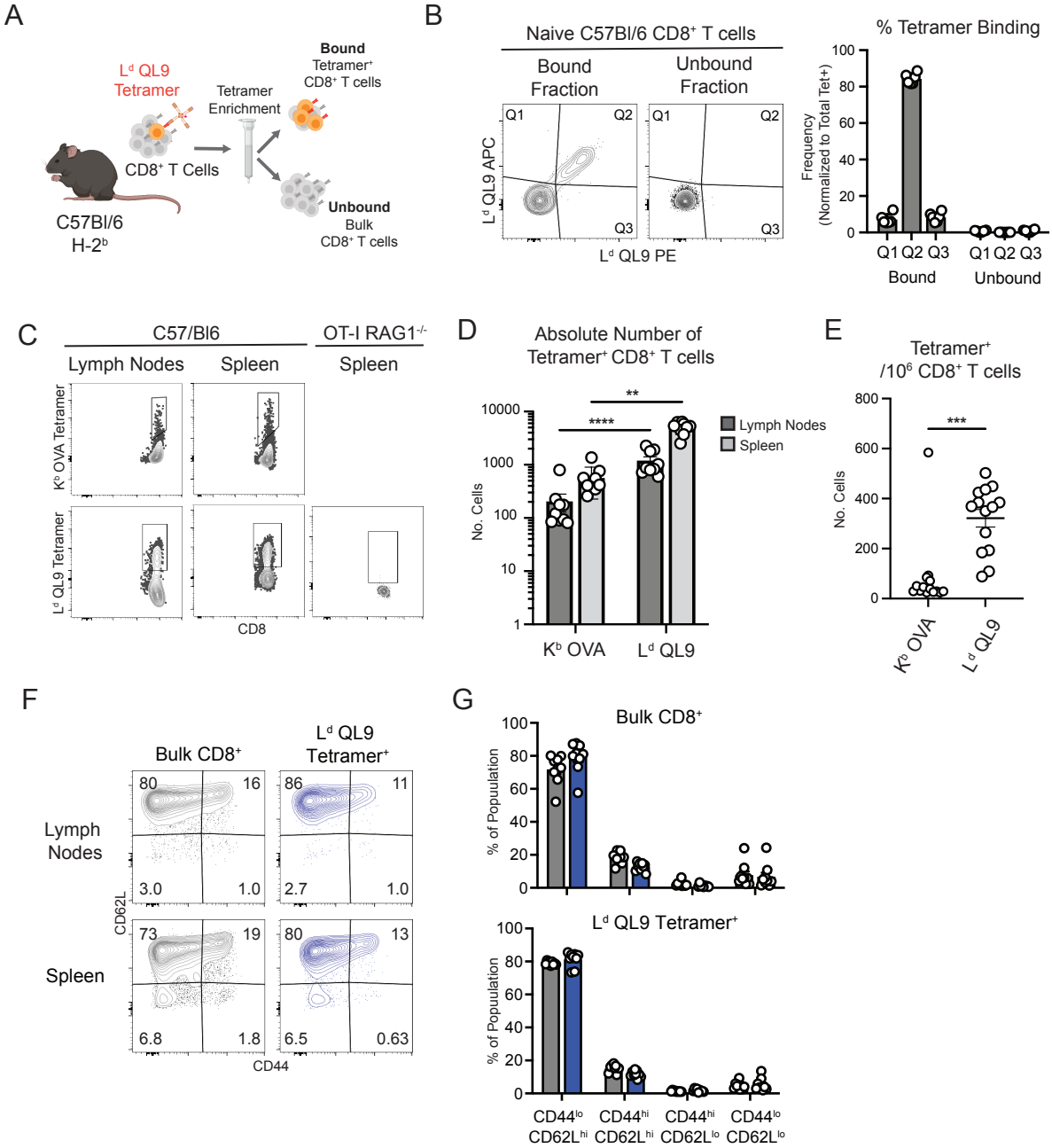
A
L^d QL9 Tetramer
Tetramer Enrichment
Bound Tetramer+ CD8+ T cells
CD8+ T Cells
Unbound Bulk CD8+ T cells
C57Bl/6 H-2^b
B
Naive C57Bl/6 CD8+ T cells
Bound Fraction
Unbound Fraction
Q1
Q2
Q3
L^d QL9 APC
L^d QL9 PE
% Tetramer Binding
Frequency (Normalized to Total Tet+)
Bound
Unbound
C
C57/Bl6
OT-I RAG1-/-
Lymph Nodes
Spleen
K^b OVA Tetramer
L^d QL9 Tetramer
CD8
D
Absolute Number of Tetramer+ CD8+ T cells
Lymph Nodes
Spleen
No. Cells
K^b OVA
L^d QL9
E
Tetramer+ /10^6 CD8+ T cells
No. Cells
K^b OVA
L^d QL9
F
Bulk CD8+
L^d QL9 Tetramer+
Lymph Nodes
Spleen
CD62L
CD44
80
16
3.0
1.0
86
11
2.7
1.0
73
19
6.8
1.8
80
13
6.5
0.63
G
Bulk CD8+
L^d QL9 Tetramer+
% of Population
CD44^lo CD62L^hi
CD44^hi CD62L^hi
CD44^hi CD62L^lo
CD44^lo CD62L^lo

Figure 2

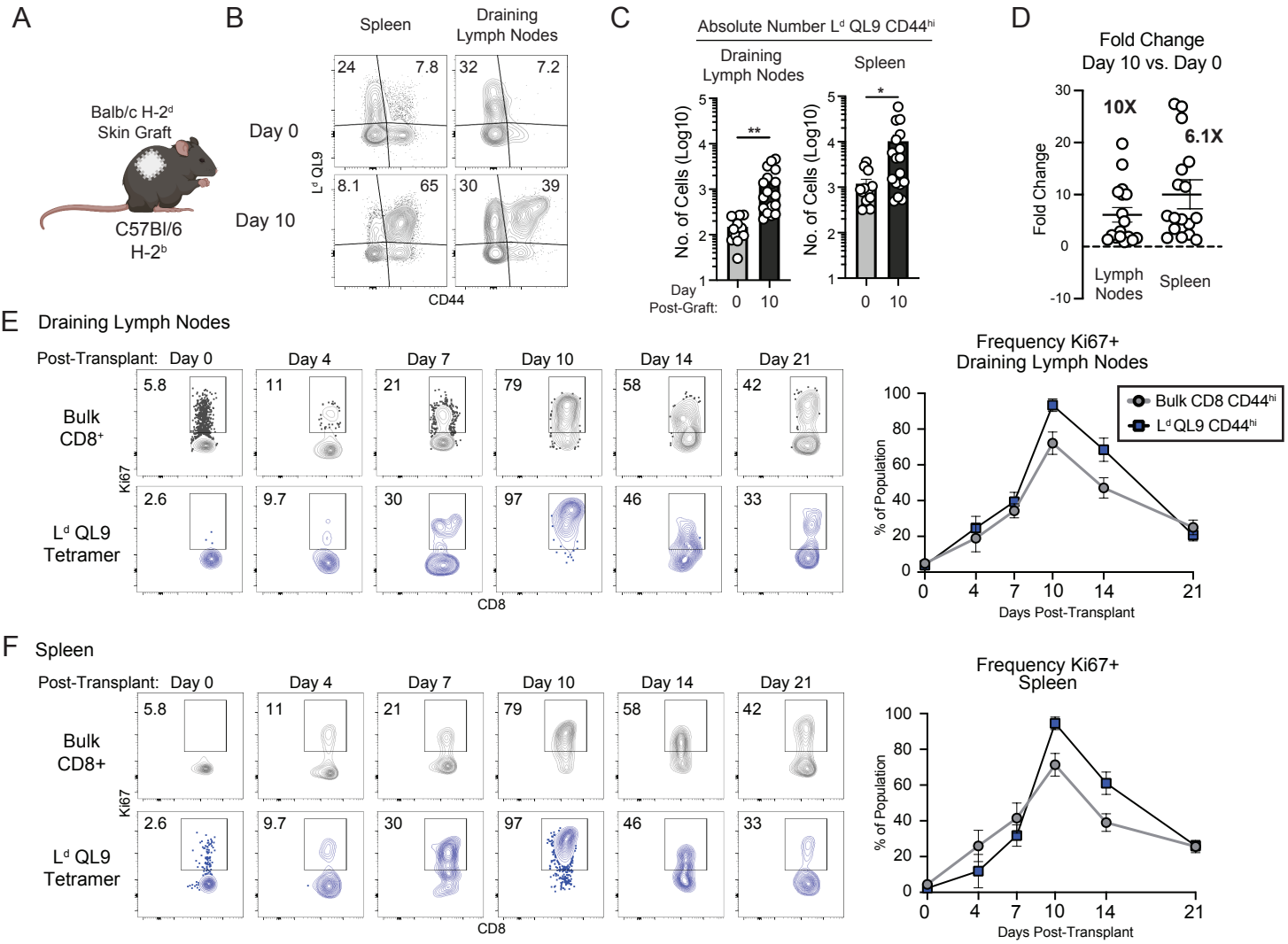
A
Balb/c H-2d
Skin Graft
C57Bl/6
H-2b
B
Spleen
Draining Lymph Nodes
Day 0
Day 10
Ld QL9
CD44
24
7.8
32
7.2
8.1
65
30
39
C
Absolute Number Ld QL9 CD44hi
Draining Lymph Nodes
Spleen
No. of Cells (Log10)
Day Post-Graft:
0
10
**
*
D
Fold Change
Day 10 vs. Day 0
Fold Change
10X
6.1X
Lymph Nodes
Spleen
E Draining Lymph Nodes
Post-Transplant: Day 0
Day 4
Day 7
Day 10
Day 14
Day 21
Bulk CD8+
Ld QL9 Tetramer
Ki67
CD8
5.8
11
21
79
58
42
2.6
9.7
30
97
46
33
Frequency Ki67+
Draining Lymph Nodes
Bulk CD8 CD44hi
Ld QL9 CD44hi
% of Population
Days Post-Transplant
F Spleen
Frequency Ki67+
Spleen

Figure 3

A

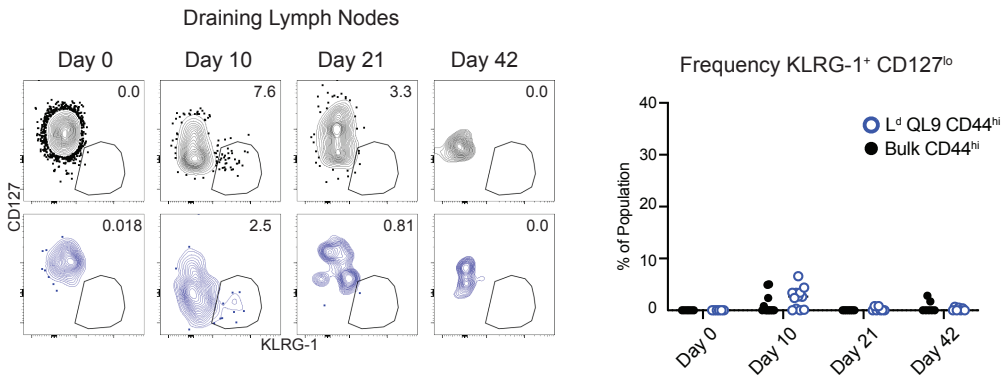
Draining Lymph Nodes
Day 0
Day 10
Day 21
Day 42
0.0
7.6
3.3
0.0
0.018
2.5
0.81
0.0
CD127
KLRG-1
Frequency KLRG-1+ CD127lo
Ld QL9 CD44hi
Bulk CD44hi
% of Population
40
30
20
10
0
Day 0
Day 10
Day 21
Day 42

B

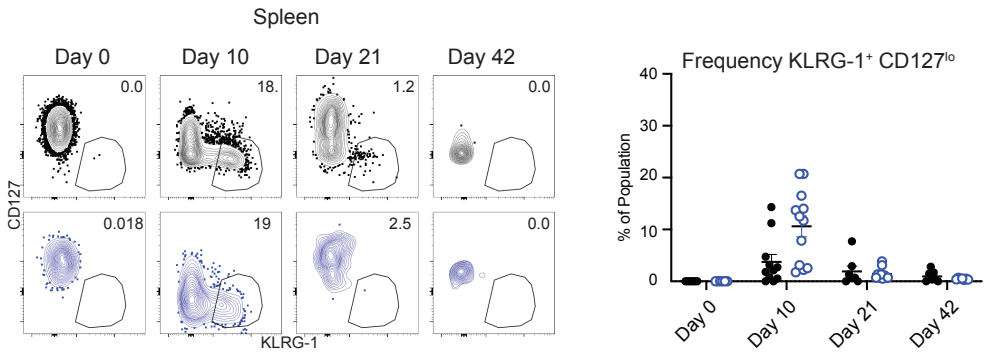
Spleen
Day 0
Day 10
Day 21
Day 42
0.0
18.
1.2
0.0
0.018
19
2.5
0.0
CD127
KLRG-1
Frequency KLRG-1+ CD127lo
% of Population
40
30
20
10
0
Day 0
Day 10
Day 21
Day 42

Figure 4

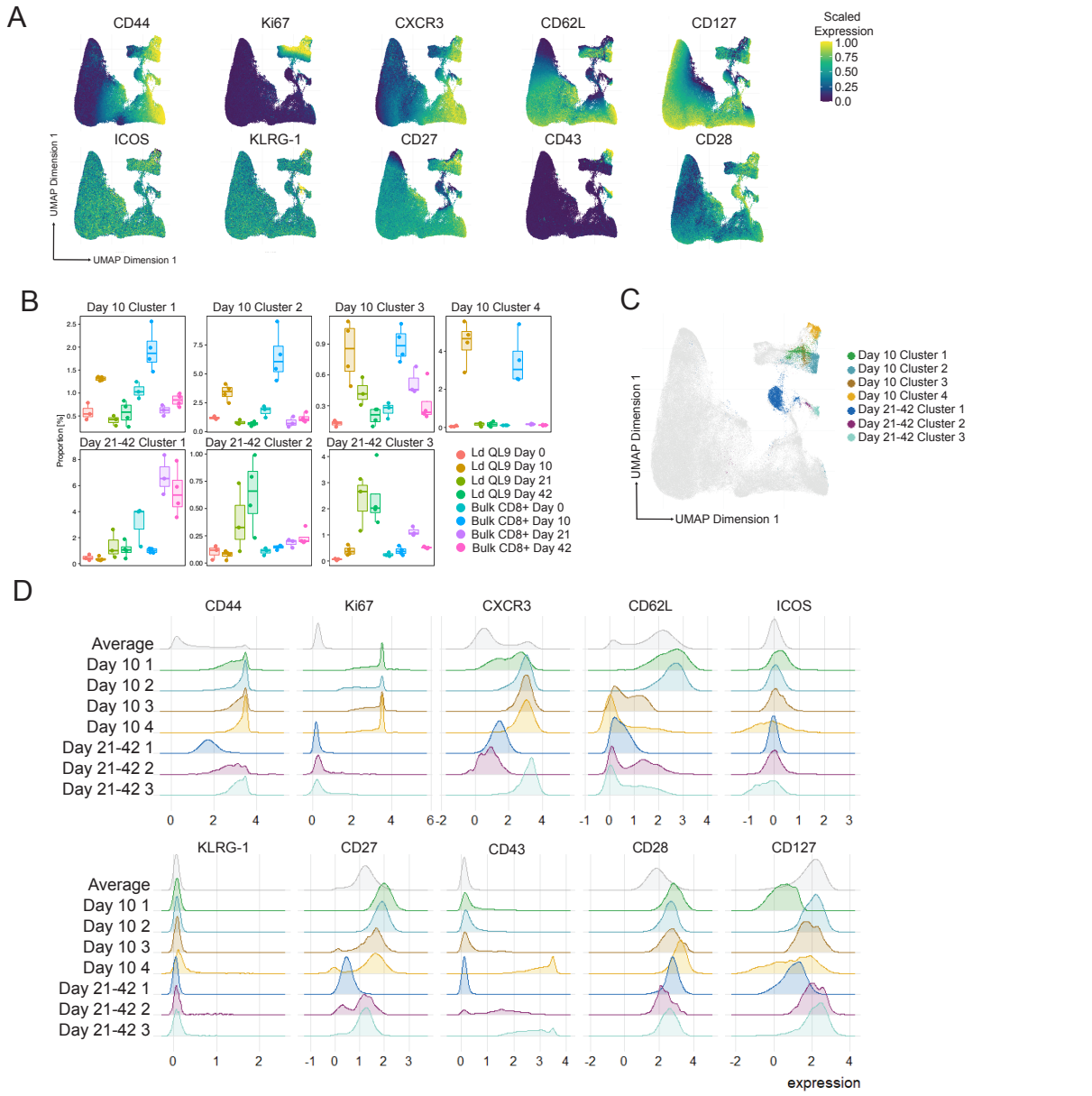
A
CD44
Ki67
CXCR3
CD62L
CD127
ICOS
KLRG-1
CD27
CD43
CD28
Scaled Expression
1.00
0.75
0.50
0.25
0.0
UMAP Dimension 1
UMAP Dimension 1
B
Day 10 Cluster 1
Day 10 Cluster 2
Day 10 Cluster 3
Day 10 Cluster 4
Day 21-42 Cluster 1
Day 21-42 Cluster 2
Day 21-42 Cluster 3
Proportion [%]
Ld QL9 Day 0
Ld QL9 Day 10
Ld QL9 Day 21
Ld QL9 Day 42
Bulk CD8+ Day 0
Bulk CD8+ Day 10
Bulk CD8+ Day 21
Bulk CD8+ Day 42
C
Day 10 Cluster 1
Day 10 Cluster 2
Day 10 Cluster 3
Day 10 Cluster 4
Day 21-42 Cluster 1
Day 21-42 Cluster 2
Day 21-42 Cluster 3
UMAP Dimension 1
UMAP Dimension 1
D
CD44
Ki67
CXCR3
CD62L
ICOS
KLRG-1
CD27
CD43
CD28
CD127
Average
Day 10 1
Day 10 2
Day 10 3
Day 10 4
Day 21-42 1
Day 21-42 2
Day 21-42 3
expression
E
CD44hi CD8+ T Cells Post-Graft
Day 0
Day 10
Day 21
Day 42
Bulk CD8+ T Cells
Ld QL9+ T Cells
CD62L
CD43
84.5
0.092
15.3
0.11
66.3
8.50
5.35
19.8
65.9
4.73
21.9
7.42
78.8
2.89
14.6
3.70
72.5
0.15
27.1
0.20
50.9
7.82
5.01
36.3
39.1
10.7
29.0
21.2
63.5
6.48
18.1
11.9
% CD62Llo CD43+
Bulk CD8+ T Cells
Ld QL9+ T Cells
% of Population
Day Post-Graft
0
10
21
42
60
40
20
0
**
*
**

Figure 5

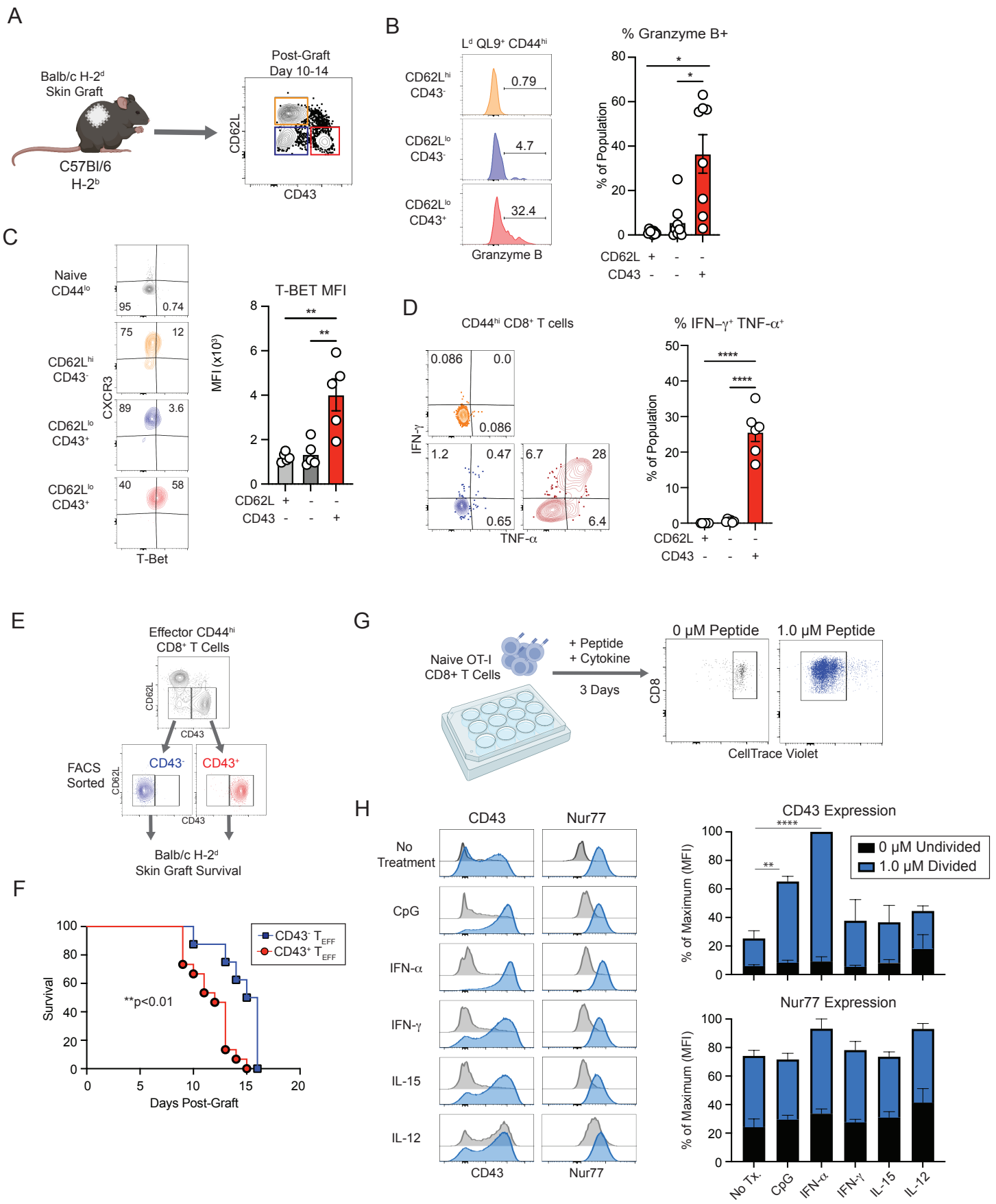
A
Balb/c H-2d
Skin Graft
C57Bl/6
H-2b
Post-Graft
Day 10-14
CD62L
CD43
B
Ld QL9+ CD44hi
CD62Lhi
CD43-
0.79
CD62Llo
CD43-
4.7
CD62Llo
CD43+
32.4
Granzyme B
% Granzyme B+
% of Population
CD62L + - -
CD43 - - +
C
Naive
CD44lo
95
0.74
CD62Lhi
CD43-
75
12
CD62Llo
CD43+
89
3.6
CD62Llo
CD43+
40
58
CXCR3
T-Bet
T-BET MFI
MFI (x10³)
CD62L + - -
CD43 - - +
D
CD44hi CD8+ T cells
0.086
0.0
0.086
1.2
0.47
0.65
6.7
28
6.4
IFN-γ
TNF-α
% IFN–γ+ TNF-α+
% of Population
CD62L + - -
CD43 - - +
E
Effector CD44hi
CD8+ T Cells
CD62L
CD43
FACS
Sorted
CD43-
CD43+
Balb/c H-2d
Skin Graft Survival
F
CD43- TEFF
CD43+ TEFF
**p<0.01
Survival
Days Post-Graft
G
Naive OT-I
CD8+ T Cells
+ Peptide
+ Cytokine
3 Days
0 μM Peptide
1.0 μM Peptide
CD8
CellTrace Violet
H
CD43
Nur77
No
Treatment
CpG
IFN-α
IFN-γ
IL-15
IL-12
CD43 Expression
0 μM Undivided
1.0 μM Divided
% of Maximum (MFI)
Nur77 Expression
No Tx.
CpG
IFN-α
IFN-γ
IL-15
IL-12

Figure 6

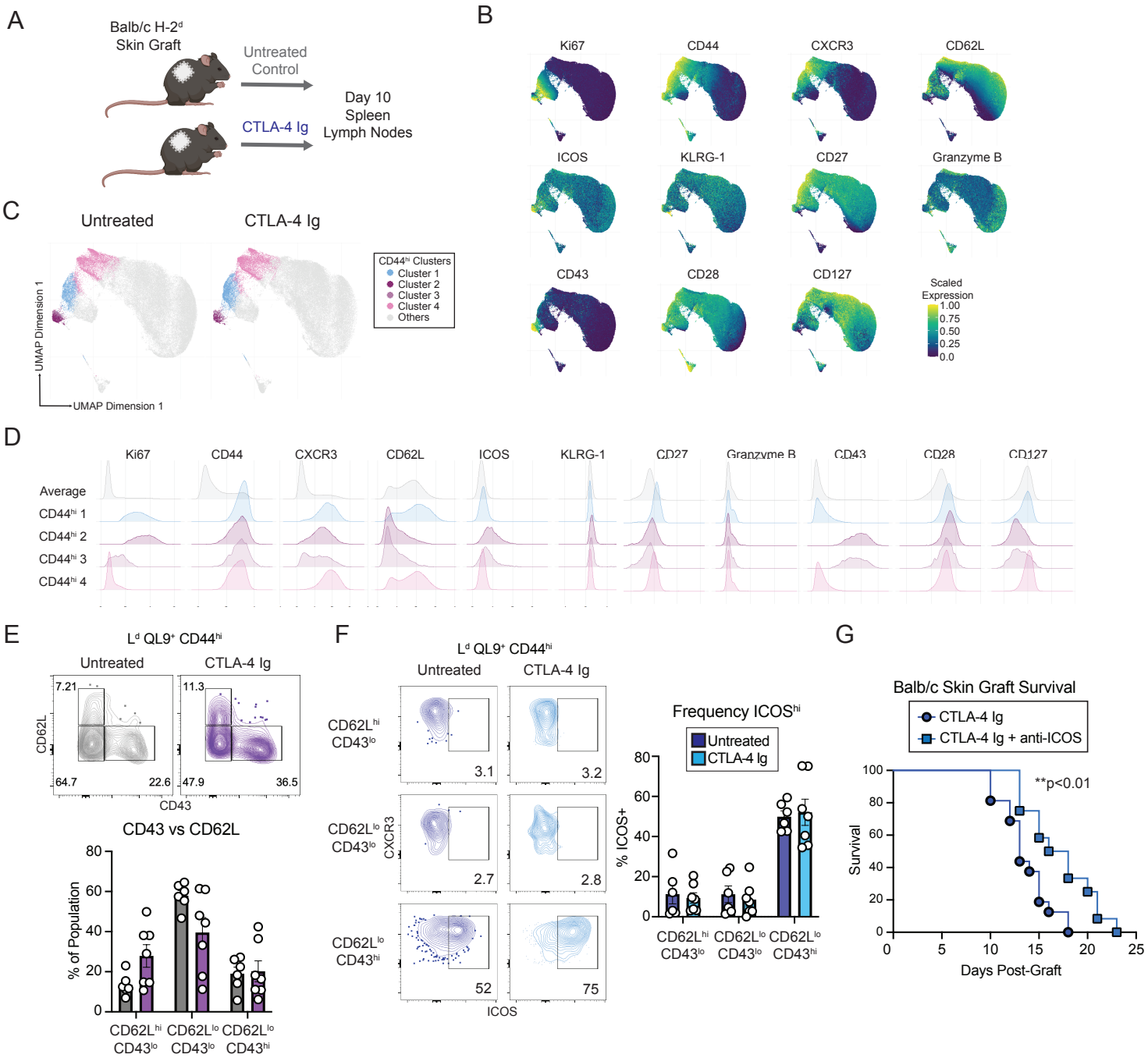
A
Balb/c H-2d
Skin Graft
Untreated
Control
CTLA-4 Ig
Day 10
Spleen
Lymph Nodes
B
Ki67
CD44
CXCR3
CD62L
ICOS
KLRG-1
CD27
Granzyme B
CD43
CD28
CD127
Scaled
Expression
1.00
0.75
0.50
0.25
0.0
C
Untreated
CTLA-4 Ig
CD44hi Clusters
Cluster 1
Cluster 2
Cluster 3
Cluster 4
Others
UMAP Dimension 1
UMAP Dimension 1
D
Ki67
CD44
CXCR3
CD62L
ICOS
KLRG-1
CD27
Granzyme B
CD43
CD28
CD127
Average
CD44hi 1
CD44hi 2
CD44hi 3
CD44hi 4
E
Ld QL9+ CD44hi
Untreated
CTLA-4 Ig
7.21
64.7
22.6
11.3
47.9
36.5
CD62L
CD43
CD43 vs CD62L
% of Population
CD62Lhi CD43lo
CD62Lo CD43lo
CD62Lo CD43hi
F
Ld QL9+ CD44hi
Untreated
CTLA-4 Ig
CD62Lhi CD43lo
CD62Lo CD43lo
CD62Lo CD43hi
CXCR3
ICOS
3.1
3.2
2.7
2.8
52
75
Frequency ICOShi
Untreated
CTLA-4 Ig
% ICOS+
CD62Lhi CD43lo
CD62Lo CD43lo
CD62Lo CD43hi
G
Balb/c Skin Graft Survival
CTLA-4 Ig
CTLA-4 Ig + anti-ICOS
**p<0.01
Survival
Days Post-Graft